



Particles II

Access the latest eBook →

11

Advanced
Optical Metrology

Particles II



EVIDENT
OLYMPUS

WILEY

Impact on Biological Systems and the Environment

This eBook is dedicated to the research of Professor David Wertheim.

In collaboration with various groups, Professor Wertheim uses confocal microscopy to analyse the impact of different types of particles on human health and the environment, with a focus on human health-hazardous particles detected with solid-state nuclear track detectors (SSNTD). Download for free, today.

EVIDENT
OLYMPUS

WILEY

High-Efficiency Graphene-Oxide/Silicon Solar Cells with an Organic-Passivated Interface

Qing Gao, Jun Yan, Lu Wan, Cuili Zhang, Zhixi Wen, Xin Zhou, Han Li, Feng Li, Jingwei Chen, Jianxin Guo, Dengyuan Song, Benjamin S. Flavel,* and Jianhui Chen*

A breakthrough in graphene-oxide/silicon heterojunction solar cells is presented in which edge-oxidized graphene and an in-plane charge transfer dopant (Nafion) are combined to form a high-quality passivating contact scheme. A graphene oxide (GO):Nafion ink is developed and an advanced back-junction GO:Nafion/n-Si solar cell with a high-power conversion efficiency (18.8%) and large area (5.5 cm²) is reported. This scalable solution-based processing technique has the potential to enable low-cost carbon/silicon heterojunction photovoltaic devices.

1. Introduction

The development of renewable energy sources is crucial if current worldwide energy demands are to be met without further destruction of the environment. For crystalline (c-Si) solar cells, this equates to a continued effort to simplify manufacturing processes, reduce production costs, and maintain or improve efficiency. c-Si solar cells occupy ≈95% of the worldwide photovoltaic (PV) market,^[1] and over 70% of this can be attributed to the aluminum back surface field (Al-BSF) cell, but its power conversion efficiency (PCE) is limited to ≈20%.^[1] More complicated and thus expensive cell designs are required in order to achieve efficiencies close to the theoretical limit of ≈29%. These

include the passivated emitter and rear cell (PERC),^[2] the silicon heterojunction (SHJ) cell,^[3] the interdigitated back contact (IBC) cell,^[4] the tunnel-oxide passivating contact (TOPCon) cell,^[5] and the heterojunction-interdigitated back contact (HJ-IBC) cell, which currently holds the PCE record for crystalline silicon solar cells at 26.7%.^[6] Fortunately, the use of composite nanomaterials as new carrier-selective contacts and passivation layers in these designs offers a solution to the complexity and cost of their

manufacture. For example, Bullock et al. recently used transition metal oxides such as molybdenum oxide in a dopant-free asymmetric heterocontact cell^[7] and Chen et al. developed an ink-based carbon nanotube-passivated charge selective contact that could be directly spin coated onto the silicon wafer, and achieved device efficiencies exceeding 22%.^[8]

The high carrier mobility ($\approx 2 \times 10^6 \text{ cm}^2 \text{ V}^{-1} \text{ s}^{-1}$) and optical transparency ($\approx 97\%$)^[9] of graphene (Gr) have made it attractive as a transparent electrode in photovoltaic technologies. In 2010, Li et al. reported a Gr/Si heterojunction solar cell with an efficiency of 1.5% and showed that a Schottky junction is formed between a single layer of Gr and n-type Si (n-Si) substrates.^[10] Ihm et al. then showed that there was direct dependence of the open-circuit voltage (V_{OC}) on numbers of graphene layers.^[11] Since then, researchers have worked to improve the performance of Gr/Si solar cells with the use of doping strategies for the Gr, dielectric interlayers, and antireflective coatings. p-type dopants such as chlorine and nitrates^[12] have been shown to enhance the built-in field and increase the PCE to ≈10% and dielectric layers including SiO₂,^[13] MoS₂,^[14] Al₂O₃,^[15] GO,^[12b] 3-hexylthiophene (P3HT),^[16] and fluorographene^[17] have all been shown to passivate interfacial defects on the n-Si surface. Brus et al. studied the current transport and stability of graphene/hydrogen- or methyl groups- (CH₃-) passivated silicon heterojunction solar cell.^[18] Furthermore, transparent materials such as MgF₂/ZnS,^[12c,19] TiO₂,^[20] PMMA^[21] have been used as antireflective coatings. For example, Shi et al. have shown that the efficiency of the Gr/Si Schottky barrier solar cells can be increased from 6.5% to 14.1% after TiO₂ coating and HNO₃ doping,^[20] and Ma et al. employed an MoS₂ interlayer as an electron blocking layer and achieved a record high PCE of 15.8%, albeit on an area of 0.03 cm².^[22]

Despite these impressive performance gains, further improvements will be difficult due to the lack of a bandgap and thus semimetal nature of Gr. As such, although Gr provides good minority carrier extraction, it is poor at blocking


Q. Gao, J. Yan, L. Wan, C. Zhang, Z. Wen, X. Zhou, J. Chen, J. Guo, D. Song, J. Chen

Hebei Key Lab of Optic-Electronic Information and Materials
College of Physics Science and Technology

Hebei University
Baoding 071002, P. R. China
E-mail: chenjianhui@hbu.edu.cn

H. Li, B. S. Flavel
Institute of Nanotechnology
Karlsruhe Institute of Technology
76344 Eggenstein-Leopoldshafen, Germany
E-mail: benjamin.flavel@kit.edu

F. Li
State Key Laboratory of Photovoltaic Materials & Technology
Yingli Green Energy Holding Co., Ltd.
Baoding 071051, P. R. China

 The ORCID identification number(s) for the author(s) of this article can be found under <https://doi.org/10.1002/admi.202201221>.

© 2022 The Authors. Advanced Materials Interfaces published by Wiley-VCH GmbH. This is an open access article under the terms of the Creative Commons Attribution License, which permits use, distribution and reproduction in any medium, provided the original work is properly cited.

DOI: 10.1002/admi.202201221

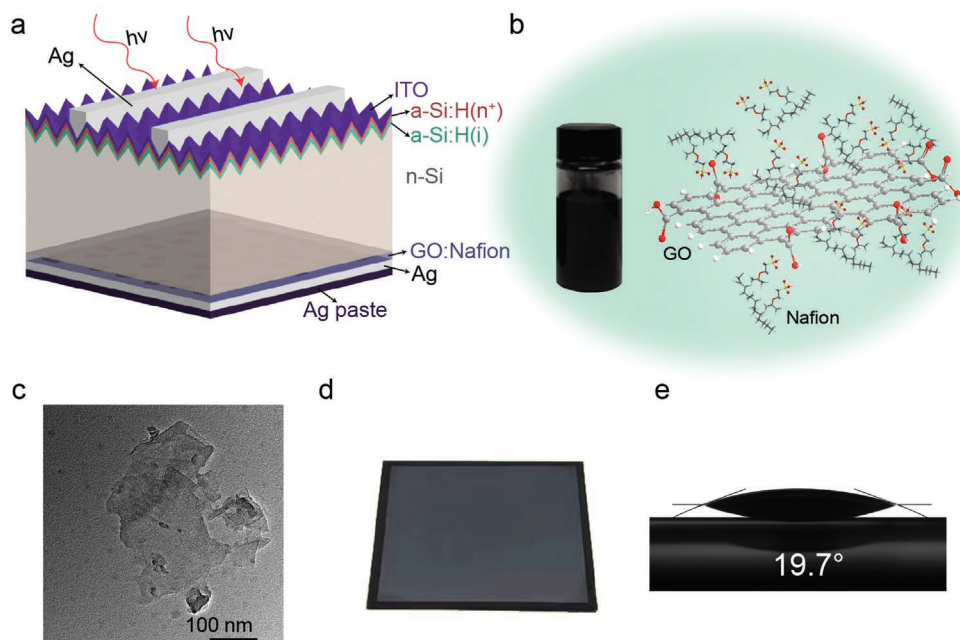


Figure 1. a) Schematic of the n-Si solar cells used in this work. b) A photograph of the GO:Nafion ink and the proposed scheme of operation involving charge transfer doping on the upper and lower layers of multilayer GO. c) A transmission electron microscopy (TEM) images and d) a photograph of a GO:Nafion coating on silicon. e) Contact angle measurement of the GO:Nafion ink on silicon.

the majority carriers at the Gr/Si metal-semiconductor (MS) heterojunction.^[12a] The oxidation of graphene, i.e., the formation of graphene oxide (GO), provides a solution to this problem and has been shown to introduce a bandgap of 0.11–4.0 eV^[23] in Gr. Nafion was reported to dope carbon electrodes effectively,^[24] exhibit a permanent doping effect in organic light-emitting diodes^[25] and organic solar cells,^[26] and passivate dangling bonds on Si wafer surface in c-Si solar cells.^[27] In this work, we therefore develop an ink of GO mixed with Nafion that can be spin coated on a n-Si wafer. Low interface recombination is provided by the Nafion and carrier selection by the GO. Using this approach, a large area (5.5 cm²) of GO:Nafion/Si solar cell with a high PCE of 18.8% is demonstrated.

2. Results and Discussion

Figure 1a shows the solar cell architecture used in this work. For the first time in the Gr/Si photovoltaic community, the GO:Nafion layer was placed on the rear of the cell in a back junction design. An electron-selective passivation contact comprising n-doped hydrogenated amorphous silicon with an ITO overlayer (ITO/a-Si:H(i/n⁺)) was used to enhance light trapping and reduce surface recombination. Shear force mixing was used to disperse 8 mg mL⁻¹ of 4–10% edge-oxidized graphene in Nafion (**Figure 1b**) and afford a GO:Nafion ink that had good wettability on silicon (**Figure 1c**). This is evidenced by the small-measured contact angle of 19.7° (**Figure 1d**) and which facilitated the formation of large-area coatings by spin coating. As a control, Gr was also shear force mixed in Nafion at concentration of 8 mg mL⁻¹. Either of these inks were then spin coated onto the back of the Si wafer, a thin film of Ag was evaporated on top of this and finally an electrical Ag paste was

applied for encapsulation and to block the ingress of small quantities of water.^[8] Atomic force microscopy (AFM) revealed that the GO:Nafion layers completely covered the Si surface and a root mean roughness of 89 nm was recorded (**Figure S1**, Supporting Information). Roughness was found to be beneficial in forming electrical contact between the GO sheets and the Ag electrode. This is because GO has good electrical conductivity and when the GO sheets are irregularly arranged, they form a good electrical point contact to the silver. In the following discussion, it will now be shown that the GO:Nafion layer simultaneously forms a p–n junction with silicon and passivates the surface defects at the GO:Si interface.

Figure 2a shows the Raman spectra of the GO, GO:Nafion, and Gr:Nafion samples. The peaks at 1341, 1571, and 2685 cm⁻¹ are D, G, and 2D modes, respectively.^[9,28] The G band is due to the E_{2g} phonon and represents sp² C=C hybridization.^[28] The D band is due to the A_{1g} symmetry,^[28] and its intensity, I_D, is associated with the amount of sp³ bonding.^[29] Therefore, the Raman spectra of the Gr:Nafion show that the Gr is mainly sp² hybridized. The presence of a G band and a D band for the GO and GO:Nafion samples indicates that oxidation is partial and is consistent with the edge-oxidation of GO. The intensity ratios of the G to 2D band, I_G/I_{2D}, for GO and GO:Nafion samples were 0.35 and 0.34, respectively, and this indicates the presence of multilayers in the GO sample.^[30] In addition, after GO was mixed with Nafion, the intensity of D band changes. The intensity ratios of D to G band (I_D/I_G) were 0.26 and 0.72 for the GO and GO:Nafion samples, respectively. This value reveals information about the sp³:sp² ratio in the sample,^[31] and indicates a chemical modification of the GO upon exposure to Nafion. As measured by ultraviolet photoelectron spectroscopy (UPS) in **Figure 2b**, this imparts a difference in the work function for the GO:Nafion and Gr:Nafion samples compared with GO alone. By taking the

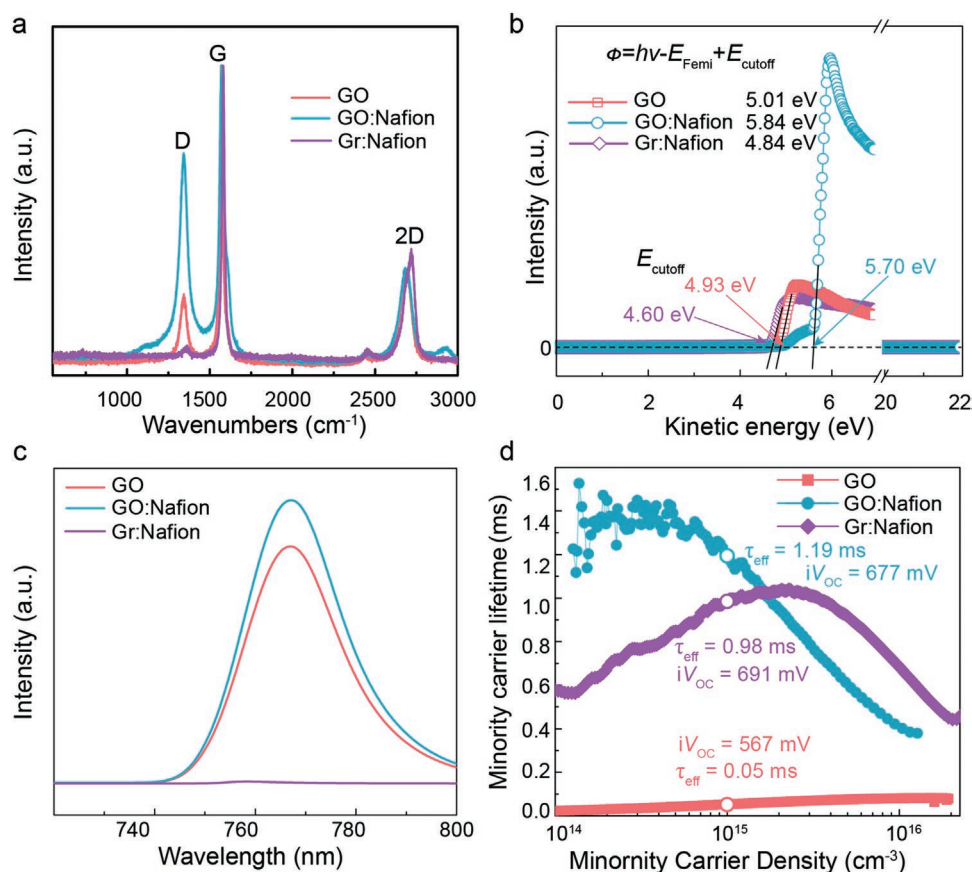


Figure 2. a) Raman-, b) ultraviolet photoelectron-, and c) photoluminescence spectra of GO, GO:Nafion, and Gr:Nafion samples. The Fermi Energy (E_{Fermi}) of GO, GO:Nafion, and Gr:Nafion films are 21.14, 21.08, 21.14 eV, respectively. d) Minority carrier lifetime measurements of thin films of these samples on an Si wafer.

inelastic electron cutoff energy (E_{cutoff}) and the Fermi level (E_{F}) of the corresponding Au calibration, the work functions of GO, GO:Nafion, and Gr:Nafion were determined to be 5.01, 5.84, and 4.84 eV, respectively. Note that the work function of the Nafion is 4.20 eV.^[27] It is clear that the work function of GO:Nafion is higher than that of GO or Nafion. This indicates that charge transfer doping has occurred in the GO:Nafion case and the reaction between the Nafion and GO is important for the work function. In addition, the work function of GO:Nafion is higher than that of Gr:Nafion. A high work function p-type material is beneficial in a p–n junction as it increases the V_{OC} and forms a high transport barrier for electrons. Photoluminescence spectra measured with an excitation wavelength of 750 nm (Figure S2, Supporting Information) shown in Figure 2c show that the bandgap of GO and GO:Nafion samples is determined to be 1.62 eV and is consistent with the results of Liang and Spanò et al.^[32]

Using the technique of the quasi-steady state and transient photoconductance decay (PCD), the minority carrier lifetimes (τ_{eff}) for silicon wafers coated with a GO film, a GO:Nafion film, or a Gr:Nafion film were measured and are shown in Figure 2d. The lifetime of GO/Si was 0.05 ms, which indicates that there is no passivation effect from GO alone. Alternatively, the lifetime of the GO:Nafion/Si and Gr:Nafion samples dramatically improved to 1.19 and 0.98 ms, and is associated with the ability of Nafion to passivate electron traps at the Si surface.^[27] This

effect is based on an electrochemical passivation mechanism, which has been explained in detail in our previous work^[27,33] and originates from the grafting of the sulfonic functional group in the Nafion molecule onto the Si surface. This high level of passivation is reflected in an increase of the implied V_{OC} (iV_{OC}) from 567 to 670 mV for the GO to GO:Nafion samples. To summarize, Nafion passivates silicon effectively whereas GO and Gr do not. Similar to our previous work on low-D:organic inks with carbon nanotubes,^[21] a conductive passivating contact is obtained.

UPS data allow for the band line-up diagrams in Figure 3a,b to be drawn. A very thin SiOR layer is formed during passivation and originates from suboxidization of Si surface-dangling bonds by the organic Nafion molecule by the electrochemical grafting O groups in the sulfonic group onto Si surface (R is the surplus O-containing constituent in the Nafion molecule).^[27] The SiOR layer is beneficial to reduce interfacial recombination and improve the effective transport of holes. GO:Nafion has a higher work function than GO and Gr:Nafion and this leads to greater band bending at the interface, the extent of which was quantified by C^{-2} - V plots at a signal frequency of 400 kHz for the GO:Nafion/Si and Gr:Nafion/Si heterojunction solar cells in Figure 3c. The GO:Nafion/Si heterojunction shows a higher (0.773 eV) built-in potential than the Gr:Nafion/Si (0.683 eV) heterojunctions. Here, despite Gr:Nafion also having excellent interfacial passivation, the lower work function

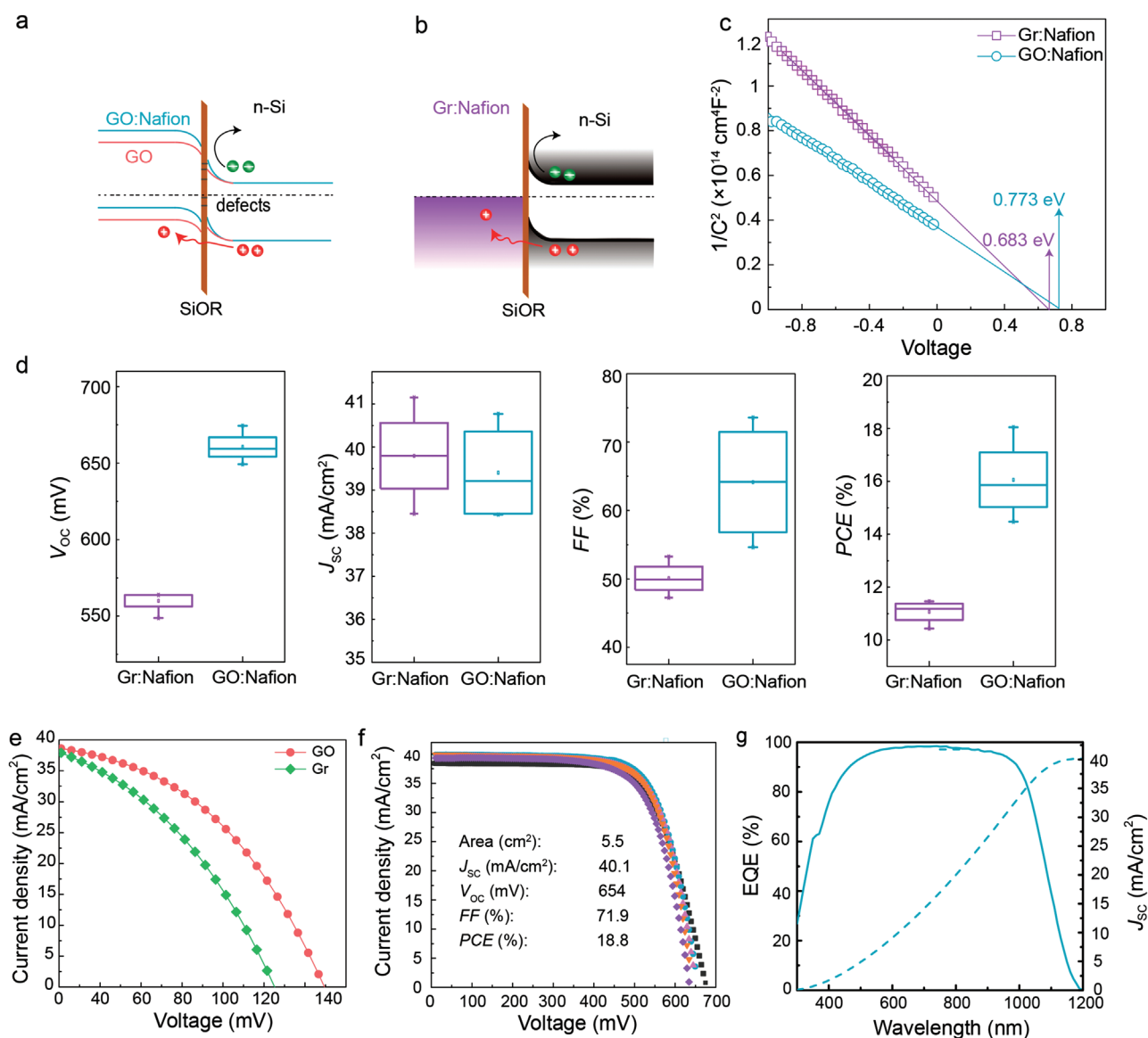


Figure 3. Band schematic diagram of: a) GO/Si and GO:Nafion/Si, and b) Gr:Nafion/Si heterojunctions. c) Capacitance–voltage measurements to determine the built-in potential, d) Gr:Nafion/Si and GO:Nafion/Si solar cell performance statistics. e) The current density–voltage (J – V) curves of Gr and GO solar cells. The powders of GO and Gr were dissolved in ethanol at 8 mg mL⁻¹, and then spin-coated at 5000 rpm under an N₂ atmosphere at room temperature. f) J – V curves and the champion photovoltaic performance parameters of GO:Nafion/Si solar cell. g) The corresponding EQE curve of the champion GO:Nafion/Si solar cell.

and thus reduced band bending limit the performance of this MS heterojunction.^[10,34] This also highlights the advantage of using edge-modified Gr for this application. As a 2D material, graphene has a work function that is determined by its grafted edges and in-plane doping. This leads to the observation that when Gr is edge is oxidized by 4–10% its work function changes from 4.68 eV (Figure S3, Supporting Information) to 5.01 eV and after Nafion doping to 5.84 eV.

In Figure 3d, a comparison of the performance of Gr:Nafion/n-Si solar cells and GO:Nafion/n-Si solar cells is shown. A lower V_{oc} and FF in the case of the Gr:Nafion/n-Si solar cells results in a lower PCE compared with the GO:Nafion devices. Gr/Si and GO/Si heterojunction solar cells without the Nafion passivation are shown in Figure 3e. Figure 3f shows an J – V curves of

GO:Nafion/Si solar cell. The dependence of the GO:Nafion ratio is also shown in Figure S4 (Supporting Information). A high PCE of 18.8% (Table S1, Supporting Information) with a V_{oc} of 654 mV, a short-circuit current density (J_{sc}) of 40.1 mA cm⁻², and a fill factor (FF) of 71.9% was achieved. Good external quantum efficiency (EQE) was demonstrated and an integrated J_{sc} of 40.1 mA cm⁻² was obtained (Figure 3g). In comparison, the Gr:Nafion/Si solar cells exhibited a lower V_{oc} (564 mV) and FF (53.54%) and this led to lower PCEs of ~11.6%. In addition, the Gr:Nafion/Si solar cells have the advantage that there is no concern about the lateral transport of the GO:Nafion composite film because the solar cell back contact is not limited by any grid.

2D photoluminescence (PL) mapping was performed on both solar cells with an area of 3 × 3 cm², Figure 4a. A homogenous

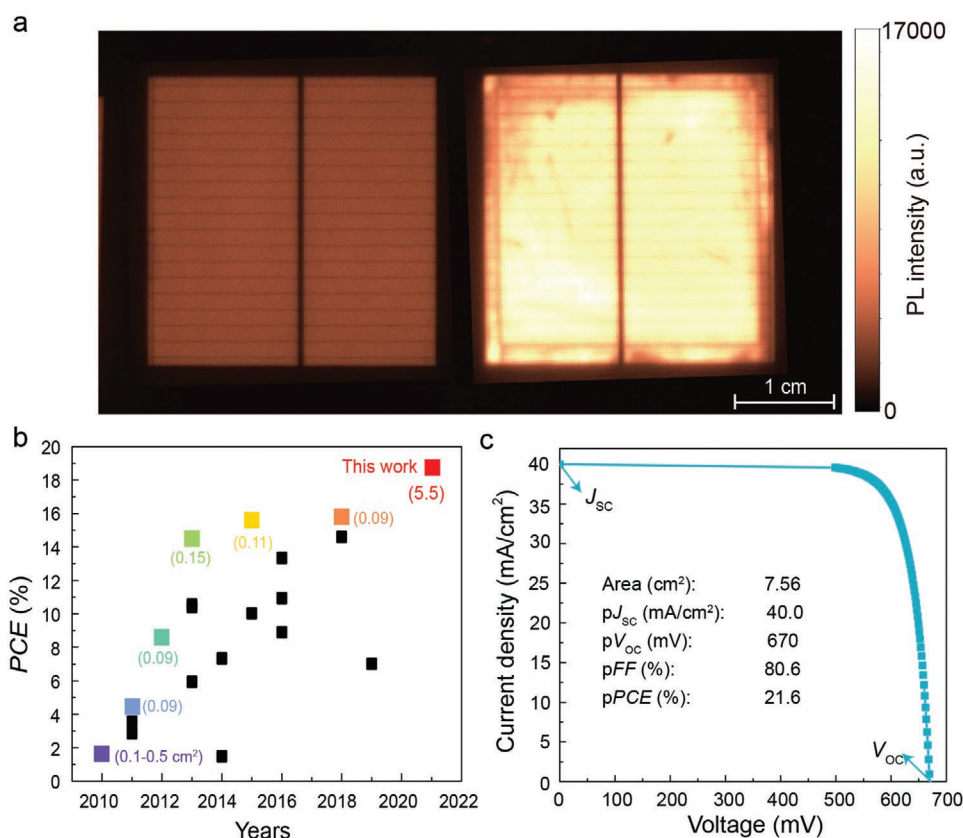


Figure 4. a) Photoluminescence intensity map of a $3 \times 3 \text{ cm}^2$ solar cell without (left) or with (right) GO:Nafion film. The thickness of GO:Nafion film is $\approx 500 \text{ nm}$ and the dark stripe in the middle of the solar cell is an Ag grid on the front side of device. b) Published efficiencies of Gr/Si solar cells with the active area indicated. c) Pseudo J - V curve and photovoltaic performance parameters for a GO:Nafion/Si solar cell.

PL contrast in both cases indicates minimal film variation across the surface, but a higher PL intensity for the GO:Nafion solar cell indicates that the Si surface defects have been more effectively passivated. Figure 4b plots the PCE of previous Gr/Si solar cells in the literature and compares them to our work. More detailed information can be found in Table S1 (Supporting Information). Not only is our device the largest but it also has the highest efficiency. In addition, compared with the previous reports,^[10,35] the solar cell architecture in our work, in which the entire wafer defines the active area, rather than a window-like design in which a carrier has to travel a distance between generation and collection at a metal contact, is of significant advantage.^[22] Pseudo J - V curve (Suns- V_{oc} measurements) in Figure 4c shows a pseudo FF (pFF) of 80.6% without the serious resistance effect, and potentially predicts that a PCE of 21.59% could be achieved with further optimization.

3. Conclusion

In conclusion, we introduce an advanced ITO/a-Si:H (i/n^+) front-contact structure to graphene-silicon solar cells and design a GO:Nafion ink that can be spin coated to form a GO:Nafion/ n -Si junction. These advancements led to solar cells with a high efficiency and device area (18.8%, 5.5 cm^2). Nafion is shown to increase the content of sp^3 hybridization in the gra-

phene lattice, facilitate charge transfer doping, and enhance the of band line-up of GO with silicon. The scalable fabrication and good wettability of the GO:Nafion ink provides a favorable direction toward development of carbon-based PV in the future.

4. Experimental Section

Solution Preparation: A Nafion solution with 10% water content was obtained by mixing an original 20 wt% Nafion (Sigma-Aldrich, 20 wt% in a mixture of lower aliphatic alcohols and 34% water) with ethanol (Sigma-Aldrich, 20 proof, anhydrous, $\geq 99.5\%$). Simple magnetic stirring for at least 4 h was used to obtain a uniform precursor solution. GO (Sigma-Aldrich, powder, 15–20 sheets, with 4–10% edge-oxidized content) was mixed in Nafion or ethanol in the ratio of 2–8 mg mL^{-1} , then the solution was shear force mixed for 3 h in order to prepare uniform solution to ensure the good reproducibility of device performances. The Gr:Nafion ink was prepared in the same way as GO:Nafion (Table S2, Supporting Information).

Solar Cells: The solar cell was fabricated using an (100)-oriented n -type CZ wafers with a thickness of about $180 \mu\text{m}$, a resistivity of about $2 \Omega \text{ cm}$, and bulk-doping concentration of about $2.4 \times 10^{15} \text{ cm}^{-3}$. The device was fabricated with several steps: 1) wet chemistry, including texturing and cleaning of wafer surface; 2) back surface polishing by covering the back with tape and using a $\text{HNO}_3/\text{HF}/\text{H}_2\text{O}$ (4:1:2) mixed solution, which was highly associated with the final GO:Nafion film morphology; 3) the formation of the front electron-selective passivating contact, antireflection layer, and metallization; 4) spin coating of GO:Nafion thin film on the relatively flat back side at 5000 rpm under N_2 atmosphere at room temperature; 5) thermal evaporation of a 300-nm full contact Ag electrode

on GO:Nafion thin film; 6) brushing Ag paste (SPI Supplies, 0 5001) on GO:Nafion/Ag (evaporation). The resistivity and thickness of Ag paste film after drying in air is 6.9 Ω cm and 3 μ m, respectively.

Characterization: The lifetime was measured by spin-coating a GO:Nafion thin film on both sides of float-zone Si wafers (280 μ m, n-type, 1–5 Ω cm) double-sided mirror-polished surfaces with Sinton WCT-120 instrument. The surface topography and roughness of GO and GO:Nafion films were measured by atomic force microscopy (MFP-3D Origin+). TEM of GO was measured with a JEOL-2100 plus HRTEM by dropping the solution into a copper mesh. The contact angles were measured by fitting a mathematical expression to the shape of the drop and then calculating the slope of the tangent to the drop at the liquid-solid-vapor (LSV) interface line (Drop Shape Analyser, DSA100, Kruss). The PL curves of the thin films on the Si wafer were carried out with an excitation wavelength of 251 nm (Hitachi F-7000), Raman spectra were obtained with Horiba LabRam HR Evolution. Solar cells were characterized by current density–voltage (J–V) measurements under standard test conditions (AM 1.5, 100 mW cm⁻² and 25 °C) and the EQE (R3011, Enlitech). J–V measurements were conducted using a solar simulator (SAN-EIXES-100S1, level AAA) and a SYSTEM SourceMeter (Keithley 2601B). The light source was calibrated by Reference Solar Cell (RS-ID4, Ser. No. 076–2014) from Fraunhofer ISE before measuring the device. PL mapping was performed with a BT imaging LIS-R1 system. Capacitance–Voltage (CV) curves were measured with an E4980A LCR Meter at room temperature. The work function of the films was measured on a Thermo Scientific ESCALab250Xi (He I, 21.22 eV) by ultraviolet photoelectron spectroscopy (UPS).

Supporting Information

Supporting Information is available from the Wiley Online Library or from the author.

Acknowledgements

Q.G. and J.Y. contributed equally to this work. The authors gratefully acknowledge support from the National Natural Science Foundation of China (61804041), Outstanding Youth Science Foundation of Hebei Province (F2019201367), Top Young Outstanding Innovative Talents Program of Hebei Province (BJ2021006), Natural Science Foundation of Hebei Province (F2019204325), National Program on Key R&D of China (2018YFB1500201), the German Research Foundation (DFG) (FL 834/2-2, FL 834/5-1, FL 834/7-1, and FL 834/9-1), Foreign Scientist Joint Research of Hebei Province (2021-16), The cooperative scientific research project of “Chunhui Program” of Ministry of Education (2018-7), and the Postgraduate Innovation Funding Project of Hebei University (HBU2021ss068).

Open access funding enabled and organized by Projekt DEAL.

Conflict of Interest

The authors declare no conflict of interest.

Data Availability Statement

The data that support the findings of this study are available from the corresponding author upon reasonable request.

Keywords

graphene, organic passivation, photovoltaic, reduced graphene oxide, silicon solar cells

Received: June 2, 2022

Revised: June 13, 2022

Published online: July 28, 2022

- [1] T. G. Allen, J. Bullock, X. Yang, A. Javey, S. De Wolf, *Nat. Energy* **2019**, *4*, 914.
- [2] B. Min, M. Müller, H. Wagner, G. Fischer, R. Brendel, P. P. Altermatt, H. Neuhaus, *IEEE J. Photovolt.* **2017**, *7*, 1541.
- [3] C. Messmer, M. Bivour, J. Schön, S. W. Glunz, M. Hermle, *IEEE J. Photovolt.* **2018**, *8*, 456.
- [4] L. Song, X. Yu, D. Yang, *J. Alloys Compd.* **2019**, *806*, 63.
- [5] A. Richter, J. Benick, F. Feldmann, A. Fell, M. Hermle, S. W. Glunz, *Sol. Energy Mater. Sol. Cells* **2017**, *173*, 96.
- [6] M. Green, E. Dunlop, J. Hohl-Ebinger, M. Yoshita, N. Kopidakis, X. Hao, *Prog. Photovolt.* **2021**, *29*, 3.
- [7] L. G. Gerling, S. Mahato, A. Morales-Vilches, G. Masmitja, P. Ortega, C. Voz, R. Alcubilla, J. Puigdollers, *Sol. Energy Mater. Sol. Cells* **2016**, *145*, 109.
- [8] J. Yan, C. Zhang, H. Li, X. Yang, L. Wan, F. Li, K. Qiu, J. Guo, W. Duan, A. Lambert, W. Lu, D. Song, K. Ding, B. S. Flavel, J. Chen, *Adv. Sci. (Weinh.)* **2021**, *8*, 2102027.
- [9] S. K. Behura, S. Nayak, I. Mukhopadhyay, O. Jani, *Carbon* **2014**, *67*, 766.
- [10] X. Li, H. Zhu, K. Wang, A. Cao, J. Wei, C. Li, Y. Jia, Z. Li, X. Li, D. Wu, *Adv. Mater.* **2010**, *22*, 2743.
- [11] K. Ihm, J. T. Lim, K.-J. Lee, J. W. Kwon, T.-H. Kang, S. Chung, S. Bae, J. H. Kim, B. H. Hong, G. Y. Yeom, *Appl. Phys. Lett.* **2010**, *97*, 032113.
- [12] a) X. Li, D. Xie, H. Park, M. Zhu, T. H. Zeng, K. Wang, J. Wei, D. Wu, J. Kong, H. Zhu, *Nanoscale* **2013**, *5*, 1945; b) L. Yang, X. Yu, M. Xu, H. Chen, D. Yang, *J. Mater. Chem. A* **2014**, *2*, 16877; c) L. Lancellotti, E. Bobeico, A. Castaldo, P. Delli Veneri, E. Lago, N. Lisi, *Thin Solid Films* **2018**, *646*, 21.
- [13] Y. Jia, P. Li, X. Gui, J. Wei, K. Wang, H. Zhu, D. Wu, L. Zhang, A. Cao, Y. Xu, *Appl. Phys. Lett.* **2011**, *98*, 133115.
- [14] X. Kong, L. Zhang, B. Liu, H. Gao, Y. Zhang, H. Yan, X. Song, *RSC Adv.* **2019**, *9*, 863.
- [15] M. A. Rehman, I. Akhtar, W. Choi, K. Akbar, A. Farooq, S. Hussain, M. A. Shehzad, S.-H. Chun, J. Jung, Y. Seo, *Carbon* **2018**, *132*, 157.
- [16] C. Xie, X. Zhang, Y. Wu, X. Zhang, X. Zhang, Y. Wang, W. Zhang, P. Gao, Y. Han, J. Jie, *J. Mater. Chem. A* **2013**, *1*, 8567.
- [17] M. Zhong, D. Xu, X. Yu, K. Huang, X. Liu, Y. Qu, Y. Xu, D. Yang, *Nano Energy* **2016**, *28*, 12.
- [18] a) V. V. Brus, M. A. Gluba, X. Zhang, K. Hinrichs, J. Rappich, N. H. Nickel, *Phys. Status Solid.* **2014**, *211*, 843; b) V. V. Brus, M. A. Gluba, X. Zhang, K. Hinrichs, J. Rappich, N. H. Nickel, *Sol. Energy* **2014**, *107*, 74.
- [19] K. Ding, X. Zhang, L. Ning, Z. Shao, P. Xiao, A. Ho-Baillie, X. Zhang, J. Jie, *Nano Energy* **2018**, *46*, 257.
- [20] E. Shi, L. Zhang, Z. Li, P. Li, Y. Shang, Y. Jia, J. Wei, K. Wang, H. Zhu, D. Wu, S. Zhang, A. Cao, *Sci. Rep.* **2012**, *2*, 884.
- [21] X. Liang, B. A. Sperling, I. Calizo, G. Cheng, C. A. Hacker, Q. Zhang, Y. Obeng, K. Yan, H. Peng, Q. Li, X. Zhu, H. Yuan, A. R. Hight Walker, Z. Liu, L.-m. Peng, C. A. Richter, *ACS Nano* **2011**, *5*, 9144.
- [22] J. Ma, H. Bai, W. Zhao, Y. Yuan, K. Zhang, *Sol. Energy* **2018**, *160*, 76.
- [23] a) H. Huang, Z. Li, J. She, W. Wang, *J. Appl. Phys.* **2012**, *111*, 054317; b) V. Coropceanu, J. Cornil, D. A. da Silva Filho, Y. Olivier, R. Silbey, J.-L. Brédas, *Chem. Rev.* **2007**, *107*, 926.
- [24] J. Chen, D. D. Tune, K. Ge, H. Li, B. S. Flavel, *Adv. Funct. Mater.* **2020**, *30*, 2000484.
- [25] S. J. Kwon, T. H. Han, T. Y. Ko, N. Li, Y. Kim, D. J. Kim, S. H. Bae, Y. Yang, B. H. Hong, K. S. Kim, S. Ryu, T. W. Lee, *Nat. Commun.* **2018**, *9*, 2037.
- [26] I. Jeon, C. Delacou, H. Okada, G. E. Morse, T.-H. Han, Y. Sato, A. Anisimov, K. Suenaga, E. I. Kauppinen, S. Maruyama, Y. Matsuo, *J. Mater. Chem. A* **2018**, *6*, 14553.

- [27] L. Wan, C. Zhang, K. Ge, X. Yang, F. Li, W. Yan, Z. Xu, L. Yang, Y. Xu, D. Song, J. Chen, *Adv. Energy Mater.* **2020**, *10*, 1903851.
- [28] C. H. Chuang, Y. F. Wang, Y. C. Shao, Y. C. Yeh, D. Y. Wang, C. W. Chen, J. W. Chiou, S. C. Ray, W. F. Pong, L. Zhang, J. F. Zhu, J. H. Guo, *Sci. Rep.* **2014**, *4*, 4525.
- [29] A. Nourbakhsh, M. Cantoro, T. Vosch, G. Pourtois, F. Clemente, M. H. van der Veen, J. Hofkens, M. M. Heyns, S. De Gendt, B. F. Sels, *Nanotechnol* **2010**, *21*, 435203.
- [30] A. Das, B. Chakraborty, A. K. Sood, *Bull. Mater. Sci.* **2007**, 31.
- [31] A. C. Ferrari, J. Robertson, *Phys. Rev. B* **2000**, *61*, 14095.
- [32] a) H. F. Liang, C. T. G. Smith, C. A. Mills, S. R. P. Silva, *J. Mater. Chem. C* **2015**, *3*, 12484; b) S. F. Spanò, G. Isgrò, P. Russo, M. E. Fragalà, G. Compagnini, *Appl. Phys. A* **2014**, *117*, 19;
- [33] a) J. Chen, K. Ge, C. Zhang, J. Guo, L. Yang, D. Song, F. Li, Z. Xu, Y. Xu, Y. Mai, *ACS Appl. Mater. Interfaces* **2018**, *10*, 44890; b) J. Chen, B. Chen, Y. Shen, J. Guo, B. Liu, X. Dai, Y. Xu, Y. Mai, *Appl. Phys. Lett.* **2017**, *111*, 191601; c) J. Chen, Y. Shen, J. Guo, B. Chen, J. Fan, F. Li, H. Liu, Y. Xu, Y. Mai, *Appl. Phys. Lett.* **2017**, *110*, 083904.
- [34] Y. Jung, X. Li, N. K. Rajan, A. D. Taylor, M. A. Reed, *Nano. Lett.* **2013**, *13*, 95.
- [35] a) L. Lancellotti, E. Bobeico, A. Capasso, M. Della Noce, T. Dikonimos, N. Lisi, P. Veneri, *2014 Fotonica AEIT Italian Conference on Photonics Technologies*, Fotonica AEIT, Naples, Italy, May **2014**; b) X. Miao, S. Tongay, M. K. Petterson, K. Berke, A. G. Rinzler, B. R. Appleton, A. F. Hebard, *Nano. Lett.* **2012**, *12*, 2745.